# TWO FLUID MODELLING OF 3D CYLINDRICAL FLUIDIZED BEDS USING KINETIC THEORY FOR ROUGH SPHERES

**Lei Yang[1], J. T. Padding[2*], J. A. M. Kuipers[1]**

[1]*Department of Chemical Engineering and Chemistry, Eindhoven University of Technology, 5600MB, Eindhoven, the Netherlands*

[2] *Process & Energy department, Delft University of Technology, 2826CA, Delft, the Netherlands*

*Email: *J.T.Padding@tudelft.nl*

**Abstract** – Cylindrical fluidized beds are mostly encountered in industry. This work involves a study of the hydrodynamics of large scale cylindrical fluidized beds. The Euler-Euler approach (two-fluid model) is considered to be the most effective for these larger scale applications. The challenge of this model incorporated with kinetic theory of granular flow (KTGF) is to establish an accurate hydrodynamic and rheological description of the solid phase. KTGF for frictional spheres developed by Yang et al. (2016) has been incorporated into our in-house two-fluid model (TFM) code for the modeling 3D cylindrical bubbling fluidized beds. For verification, a comparison of the present model in the limit of zero friction with the original (frictionless) KTGF model is made. Simulation results of both models agree well. Numerical tests on bubbling fluidized beds are carried out using present KTGF and the KTGF model from Jenkins and Zhang (2002). The simulation results show good agreement with the simulation results obtained from the KTGF model from Jenkins and Zhang for solids circulation pattern and solids volume fraction distribution. In addition, a comparative study has been performed to investigate the effects of inlet gas velocity on bubble behavior in fluidized beds.

## INTRODUCTION

Flows of dense assemblies of granular materials are encountered in many industrial devices, such as hoppers, rotary blenders, fluidized beds, circulating fluidized beds (CFBs), spouted beds, etc. In many of these applications, there exists a two-phase flow problem. Thus, understanding and modeling gas-particle flows involving dense assemblies of particles is of significant scientific and technological interest. As is reported by Forterre and Pouliquen (2008), granular flows are often categorized into three different regimes: a dense quasi-static regime in which the deformations are very slow and the particles interact by frictional contacts (Roux and Combes, 2002); a gaseous regime in which the flow is very rapid and dilute, and the particles interact by collision (Goldhirsch, 2003); and an intermediate liquid regime in which the material is dense but still flows like a liquid, the particles interacting both by collision and friction (Pouliquen and Chevoir, 2002). Among these regimes, the last liquid regime is most often encountered in applications.

It is well known that the fluidized beds have high efficiencies in particle mixing and particle-fluid heat and mass transfer (Gilliland and Mason, 1949). Understanding the dynamics of fluidized beds is a key issue in improving efficiency, reliability and scale-up from laboratory models. The Euler-Euler approach (Kuipers et al., 1992, Gidaspow, 1994, Lu et al., 2003) is considered to be the most effective for large scale simulations. The so-called two-fluid model (TFM) incorporated with kinetic theory of granular flow (KTGF) has been widely used. In the dense gas-solid fluidization processes, the particles interact with each other through enduring frictional contact between multiple neighbors and, to a lesser extent, through collisions. In many cases, as pointed by Srivastava and Sundaresan (2003), gravity is sufficient to ensure that frictional interactions have a significant contribution to the particulate stress. As the particle volume fraction decreases, the collisional stress becomes more dominant. In these systems, the contributions from the frictional stresses and kinetic stresses are comparable. Thus, it is of significant interest to synthesize rheological KTGF models that combine the frictional and kinetic contributions.

In addition, after a binary collision between rough particles, the particles can rotate due to surface friction. Thus, translational kinetic energy may exchange with rotational kinetic energy. In addition to the mass and momentum equations, there is the requirement of an additional equation for the particle spin. Attempts to quantify this friction effect have been somewhat limited. Yang et al. (2016a) derived a kinetic theory of granular ow (KTGF) for frictional spheres using the Chapman-Enskog method in dense systems. On the one hand, this theory considers both frictional and kinetic contributions. On the other hand, it includes the effects of particle rotation and surface friction explicitly. Later, the theory was validated by Yang et al. (2016b) for the simulation of a dense gas-solid bubbling fluidized bed.

There are many experimental and computational studies reported in literature in pseudo two dimensional (2D) and purely 2D beds (Taghipour et al, 2005; Yang et al, 2016c). However, on the one hand, restricting the computational domain to two dimensions assumes an infinitely long span, an assumption which is questionable because most experimental data has been obtained from thin fluidized beds due to the validity of optical accessibility. On the other hand, wall effects (particularly the particle wall friction) play a critical role in the bubble dynamics (Li et al., 2010) in pseudo-2D laboratory and small-scale experiments. A comparison by Li et al. (2010) clearly shows that there are marked differences between two-dimensional and three-dimensional simulation predictions. Those from the three-dimensional simulations match the experimental results significantly better than those from the two-dimensional simulations. So far, the flow characteristics achieved for three dimensional (3D) fluidized beds were mostly compared with 2D or pseudo 2D systems. Cranfield and Geldart (1974) also reported that 2D simulations may yield significantly different results compared with 3D simulations. Clearly, the most widely used bed geometries in industry are 3D. So far, detailed 3D studies are rarely found in the literature because of high computational cost (Bakshi et al. 2014). From an experimental point of view, flow visualization and measurements are difficult to perform in 3D.

The present work is concerned with further validation of the rough sphere KTGF in a cylindrical bed. The present model is first incorporated into our in-house Euler-Euler code using 3D cylindrical coordinates. For verification of the implementation, a comparison of the present model in the limit of zero friction with the original (frictionless) KTGF model is made. Then, we turn to the frictional model and investigate the effect of different inlet gas velocities on the bed hydrodynamics.

## NUMERICAL MODELS

The balance equations of the new KTGF model, including full expressions for the constitutive equations, are given in Table 1. In this work, the particles have rotational degrees of freedom. During particle collisions not only linear momentum is transferred but also angular momentum. Details of the KTGF model can be found in Yang et al. (2016a). Details about implementation of the cylindrical coordinate system can be found in Verma et al. (2013).

Table. 1: Balance equations and constitutive equations for the frictional KTFG model. Here $A_1$, $A_2$, $A_3$, $A_4$ are integrals of trigonometric functions, and $\lambda = 5\Theta_r / 2\Theta_t$ is the ratio of rotational to translational granular temperature. Other variables can be found in Yang et al., 2016a.

Balance equations for fluid (*f*) and solid (*s*):

$$\frac{\partial(\varepsilon_f \rho_f)}{\partial t} + \frac{\partial}{\partial \mathbf{r}} \cdot (\varepsilon_f \rho_f \mathbf{v}_f) = 0 \tag{1}$$

$$\frac{\partial(\varepsilon_f \rho_f \mathbf{v}_f)}{\partial t} + \nabla \cdot (\varepsilon_f \rho_f \mathbf{v}_f \mathbf{v}_f) = -\varepsilon_f \nabla P_f - \nabla \cdot (\varepsilon_f \boldsymbol{\tau}_f) + \varepsilon_f \rho_f \mathbf{g} - \beta_A (\mathbf{v}_f - \mathbf{v}_s) \tag{2}$$

$$\frac{\partial(\varepsilon_s \rho_s \mathbf{v}_s)}{\partial t} + \nabla \cdot (\varepsilon_s \rho_s \mathbf{v}_s \mathbf{v}_s) = -\nabla \cdot (P_s \mathbf{I} + \varepsilon_s \boldsymbol{\tau}_s) + \varepsilon_s \rho_s \mathbf{g} + \beta_A (\mathbf{v}_f - \mathbf{v}_s) - \varepsilon_s \nabla P_f \tag{3}$$

$$\frac{3}{2}\left[\frac{\partial(\varepsilon_s \rho_s \Theta_t)}{\partial t} + \nabla \cdot (\varepsilon_s \rho_s \mathbf{v}_s \Theta_t)\right] = -\nabla \mathbf{v}_s : (P_s \mathbf{I} + \varepsilon_s \boldsymbol{\tau}_s) - \varepsilon_s \nabla \cdot (-\kappa_t \nabla \Theta_t) - \gamma_t - 3\beta_A \Theta_t \tag{4}$$

$$\frac{3}{2}\left[\frac{\partial(\varepsilon_s \rho_s \Theta_r)}{\partial t} + \nabla \cdot (\varepsilon_s \rho_s \mathbf{v}_s \Theta_r)\right] = \varepsilon_s \nabla \cdot (\kappa_r \nabla \Theta_r) - \gamma_r \tag{5}$$

Solid pressure tensor: $\mathrm{P}_s = \varepsilon_s \rho_s \Theta_t \left[1 + 2(1+e)\varepsilon_s g_0\right]$

Solid bulk viscosity: $\lambda_s = \frac{4}{3}\varepsilon_s \rho_s \sigma g_0 (1+e)\sqrt{\frac{\Theta_t}{\pi}}$

Solid stress tensor: $\boldsymbol{\tau}_s = -\left\{(\lambda_s - \frac{2}{3}\mu_{t_s})(\nabla \cdot \mathbf{v}_s)\mathbf{I} + \mu_{t_s}[\nabla \mathbf{v}_s + (\nabla \mathbf{v}_s)^T] + \mu_{r_s}[\nabla \mathbf{v}_s - (\nabla \mathbf{v}_s)^T]\right\}$

Translational energy dissipation rate:

$$\gamma_t = g_0\rho_s\Theta_t\varepsilon_s^2\left\{\begin{array}{l}-\dfrac{192}{\sigma}\sqrt{\dfrac{\Theta_t}{\pi}}\left[\eta_1(1+\eta_1)-(2\lambda+1)\mathrm{A}_1+(\lambda+1)\mathrm{A}_2\right]\\ +12\nabla\cdot\mathbf{v}_s\left[\eta_1(1+\eta_1)+5[(\lambda+1)\mathrm{A}_4-(2\lambda+1)\mathrm{A}_3\right]\end{array}\right\}$$

Rotational energy dissipation rate:

$$\gamma_r = g_0\rho_s\Theta_t\varepsilon_s^2\left\{-\frac{96}{\sigma}\sqrt{\frac{\Theta_t}{\pi}}\left(2.5\mathrm{A}_2-\lambda\mathrm{A}_1\right)+120\nabla\cdot\mathbf{v}_s\left(2.5\mathrm{A}_4-\lambda\mathrm{A}_3\right)\right\}$$

Shear viscosity: $\mu_{t_s} = \bar{\mu}(1+\mu_{t_{s,c}})+\frac{3}{5}\lambda_s,\quad \mu_{t_{s,c}} = -\frac{4}{5}\varepsilon_s g_0\left[-6(2\lambda+1)\mathrm{A}_1+2\eta_1\right]$

Rotational viscosity: $\mu_{r_s} = -8(2\lambda+1)\sigma g_0\rho_s\varepsilon_s\mathrm{A}_1\sqrt{\dfrac{\Theta_t}{\pi}}$

Pseudo translational thermal conductivity:

$$\kappa_t = \bar{\kappa}_t\left(1+\kappa_{t_{s,c}}\right)+\frac{3}{2}\lambda_s,\ \kappa_{t_{s,c}} = -\varepsilon_s g_0\left[2\eta_1-16(2\lambda+1)\mathrm{A}_1\right]$$

Pseudo rotational thermal conductivity: $\kappa_r = \bar{\kappa}_r\left(1+\kappa_{r_{s,c}}\right),\ \kappa_{r_{s,c}} = 16\lambda(\lambda+1)g_0\varepsilon_s\dfrac{\Theta_t}{\Theta_r}\sqrt{\dfrac{\Theta_t}{\pi}}\mathrm{A}_1$

Radial distribution function at contact (Ma and Ahmadi, 1986):

$$g_0 = 1+4\varepsilon_s\frac{1+2.5\varepsilon_s+4.5904\varepsilon_s^2+4.515439\varepsilon_s^3}{\left[1-\left(\varepsilon_s/\varepsilon_s^{\max}\right)^3\right]^{0.67802}}$$

## RESULTS AND DISCUSSION

### *Initial conditions and parameter settings*

In the simulations, no-slip boundary conditions for the cylindrical side walls are used for the gas phase. At the bottom inlet a uniform gas velocity is specified, whereas at the top outlet atmospheric pressure (101,325 Pa) is prescribed. For the solid phase, partial slip boundary conditions derived by Yang et al. (2016c) are used on side walls. A periodic BC is applied for flow crossing the azimuthal boundary θ=0 and θ=2π. The Euler-Euler simulations with particle and domain properties are listed in Table 2.

Table. 2: Properties of particle and settings for model validation.

| Parameters | Values |
|---|---|
| Particle | glass beads, alumina |
| Particle density, kg/m$^3$ | 2526.0 (glass), 1040 (alumina) |
| Particle diameter σ (mm), | 1.0 (glass), 1.5 (alumina) |
| Initial bed height | AR (aspect ratio) =1 |
| Grid number (r × θ × z ) | 10 × 10 × 50 (glass), 20 × 25 × 120 (alumina) |
| Normal restitution coefficient, *e* | 1.0 (glass), 0.74 (alumina) |
| Friction coefficient, $\mu$ | 0.0 (glass), 0.2 (alumina) |
| Simulation time | 20 s (glass), 10 s (alumina) |
| Minimum fluidization velocity, $U_{mf}$ , m/s | 0.636 (glass), 0.527 (alumina) |
| Superficial gas velocity, $U_g$, m/s | 2.0 (glass); 0.83, 0.99, 1.32 (alumina) |
| Flow solver time-step | $10^{-4}$ s |

### *Perfectly elastic particles*

First, tests are carried out to verify our implementation for perfectly elastic glass bead (σ=1.0 mm). Next, we investigate the influence of the particle friction for inelastic alumina beads (σ=1.5 mm). Without friction and rotation, the new KTGF is the same as the original one when the normal restitution coefficient is 1. The simulation settings are specified in Table 2. Comparisons of bed height, pressure drop, granular temperature and solids volume fraction are made in Figs. 1-2. There exist small differences between the original and the

new KTGF models. On the one hand, these small deviations are possibly due to accumulated numerical round-off errors. On the other hand, during the simulation, however, walls with gradient boundary condition is applied for the translational granular temperatures, which may contribute to these small difference. Nevertheless, we can find almost the same fluctuations in both simulations, which validates the implementation of the new model in the code for ideal particles.

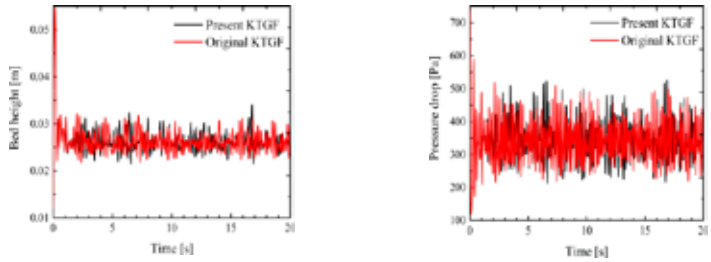


(a) Averaged bed height (b) Pressure drop in the bed

Fig. 1. Bed expansion and pressure drop with perfectly elastic glass.

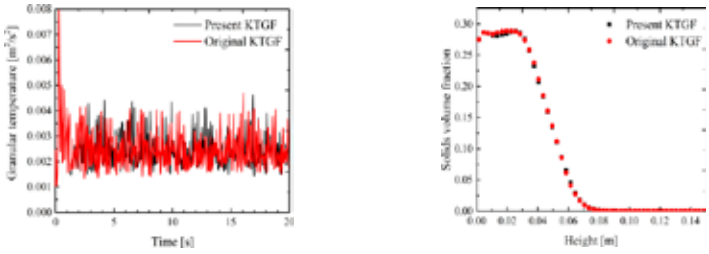


(a) Global granular temperature (b) Azimuthally and time-averaged solids distribution

Fig. 2. Global granular temperature and solids distribution over height with perfectly elastic glass.

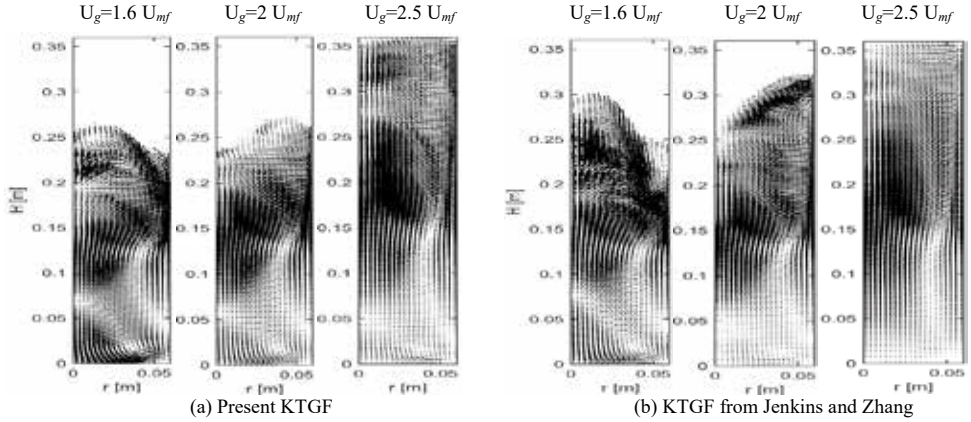


(a) Present KTGF (b) KTGF from Jenkins and Zhang

Fig. 3. Azimuthally and time-averaged solids circulation pattern predicted from simulations.

*Inelastic particles*

Next, we carry out different simulations for inelastic frictional particles (alumina beads) based on different models, i.e. the effective model from Jenkins and Zhang (2002) and our present model. First, the time-averaged solids circulation pattern is shown in Fig. 3. At low superficial gas velocity, as can be seen from both simulations, at the bottom of the bed, particles fall down in the central region while they move up close to the walls. In the upper part of the bed, the direction of particle movement is completely opposite of the one in the bottom region. This can be due to the fact that the bubbles formed at the bottom and close to the wall do not

traverse all the way to the center, producing a downward movement of the particles in the center of the bed, while these bubbles coalesce at the intermediate height above the distributor surface and afterwards, move upward. Consequently, this type of bubble behavior induces two distinct vortices in the bed. With increasing superficial gas velocity, the lower vortex shrinks while the higher vortex grows in both KTGF models. Similar influence of superficial gas velocity on solids circulation was also found by Laverman et al. (2012). However, it can be observed that the lower vortex predicted by the original KTGF disappears quicker than the one predicted by the present KTGF model.

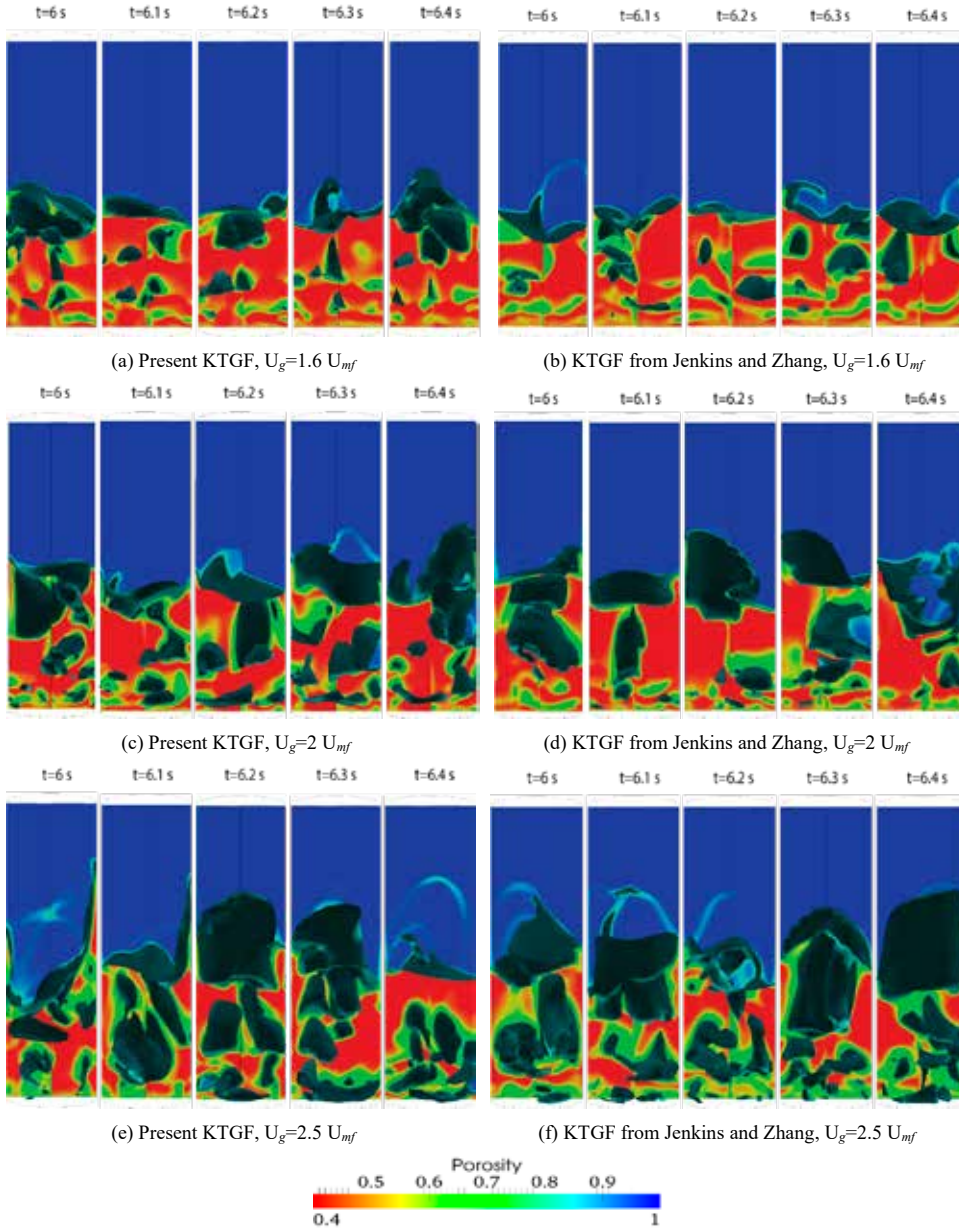


(a) Present KTGF, $U_g$=1.6 $U_{mf}$ (b) KTGF from Jenkins and Zhang, $U_g$=1.6 $U_{mf}$

(c) Present KTGF, $U_g$=2 $U_{mf}$ (d) KTGF from Jenkins and Zhang, $U_g$=2 $U_{mf}$

(e) Present KTGF, $U_g$=2.5 $U_{mf}$ (f) KTGF from Jenkins and Zhang, $U_g$=2.5 $U_{mf}$

Fig. 4. Instantaneous snapshot of gas fraction in the middle of the bed and 3D contours (dark green color, $\varepsilon_g$=0.8).

Figs. 4 and 5 show instantaneous snapshots of azimuthal and r-θ plane gas fraction at different superficial gas velocities, illustrating the bubble behavior from the wall to the central region while they are rising along the bed. At $U_g$=1.6 $U_{mf}$, small bubbles are formed at the distributor surface and close to the wall. From the contour plots, in comparison with the KTGF model from Jenkins and Zhang, more bubbles are produced in the present KTGF model. Both models predict quite homogenous bed structure. At $U_g$=2 $U_{mf}$, it is clear that more bubbles are captured by both models, and the bubble size increases compared with the simulations at $U_g$=1.6 $U_{mf}$. For $U_g$=2.5 $U_{mf}$, the bed expands rigorously and slugging fluidization occurs. Besides, as can be seen from Figs 4(e-f) and 5, the present KTGF model predicts a more heterogeneous bed structure in comparison with the KTGF model from Jenkins and Zhang. Overall, an increase in the fluidization velocity drives the bubbles formed at walls to reach centerline at lower height of the bed, and then bubbles coalesce. Thereby, the size of vortices formed in the bottom of the bed is decreased. Since the dense bed height grows by increasing the fluidization velocity, top vortices will be elongated more. Further, the increased superficial gas velocity intensifies bubble coalescence, and signifies lateral movement of the bubble near the distributor, which induces further shrinkage of lower vortices and elongation of the upper ones. All of these corresponds to the solids circulation pattern in Fig. 3.

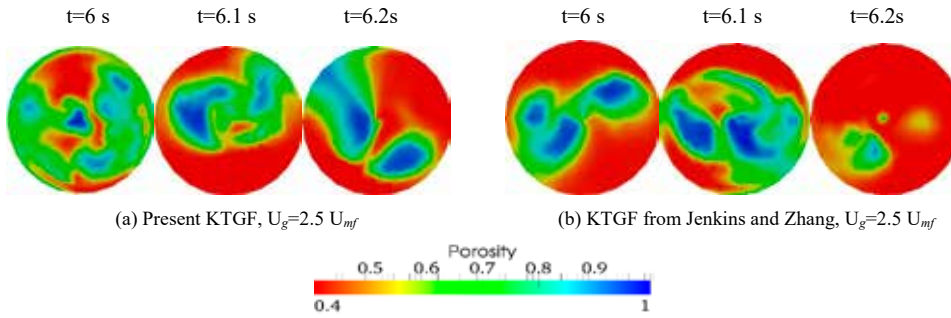


(a) Present KTGF, $U_g$=2.5 $U_{mf}$ (b) KTGF from Jenkins and Zhang, $U_g$=2.5 $U_{mf}$

Fig. 5. Instantaneous snapshot of gas fraction in r-θ plane at height H=0.1 m predicted obtained from simulations.

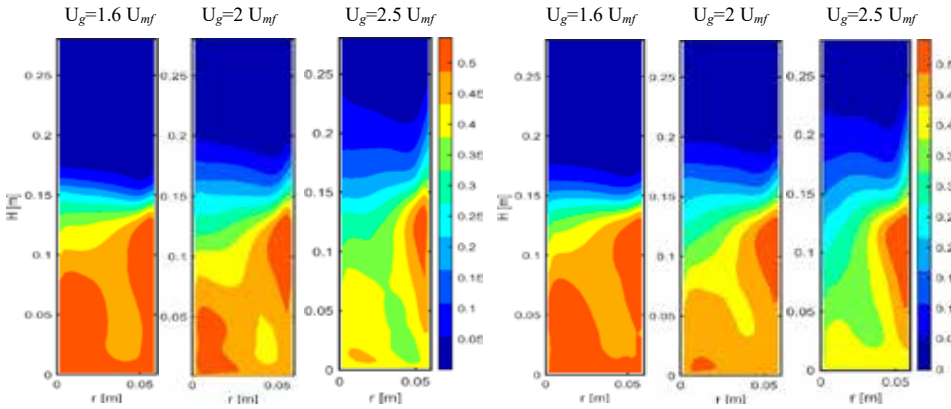


(a) Present KTGF (b) KTGF from Jenkins and Zhang

Fig. 6. Time-averaged solids volume fraction distribution obtained from simulations.

The time-averaged solids volume fraction obtained from TFM simulations are compared in Fig. 6 and Fig. 7. All profiles are qualitatively similar at different superficial gas velocities. At low superficial gas velocity, zones with high solids volume fraction near the lateral walls and bottom of the bed are observed in both TFM models, while this dense region is only found close to the lateral walls at high superficial gas velocity. Fig. 7 shows the laterally averaged solids volume fraction as a function of height. For the different superficial gas velocities similar contour shapes are obtained from both TFM simulations. At the height from 0.03-0.12 m, the present KTGF model predicts slightly higher solids concentration. At height above 0.12m, almost the same solids concentration is obtained from both models. Thus, for this case, the present KTGF model shows only a slight

difference in comparison with the KTGF model from Jenkins and Zhang regarding to the solids fraction distribution.

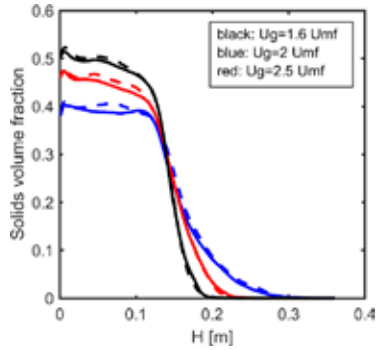


Fig. 7. Profiles of the time-averaged and laterally averaged solids volume fraction versus height obtained from simulations, dashed line: simulation results from present KTGF, line: simulation results from present KTGF.

## CONCLUSION

We have implemented the kinetic theory for rough spheres derived by Yang et al. (2016a) in three dimensional cylindrical coordinates. This implementation is first verified by comparison between the new model and the original KTGF code using the same boundary conditions for the case of perfectly elastic particles. The simulation results indicates that the implementation of the presented model is right. Besides, the present KTGF and the KTGF from Jenkins and Zhang (2002) are applied to investigate the effect of superficial gas velocity. Results show that our present KTGF can obtain close agreement with Jenkins and Zhang's KTGF model, especially for the solids volume fraction distribution. However, with increasing superficial gas velocity, we found that the lower vortex predicted by Jenkins and Zhang's KTGF disappears quicker than the one predicted by present KTGF model. Besides, the present KTGF predicts more bubbles in the bed and larger bubble size in comparison with Jenkins and Zhang's KTGF, which leads to slightly different solids circulation patterns.

## ACKNOWLEDGMENTS

The authors thank the European Research Council for its financial support, under its Advanced Investigator Grant scheme, contract no. 247298 (Multi-scale Flows).

## NOTATION

| | | | |
|---|---|---|---|
| $\mathbf{v}$ | velocity,m/s | $\kappa$ | thermal conductivity, kg/(m·s) |
| $\Theta$ | granular temperature, $m^2/s^2$ | $\boldsymbol{\omega}$ | rotational velocity, rad/s |
| $\beta_0$ | tangential restitution coefficient | $\mathbf{F}$ | force, N |
| $\varepsilon$ | volume fraction | $\boldsymbol{\tau}$ | stress tensor, Pa |
| $\sigma$ | particle diameter, m | $\gamma$ | energy dissipation rate, kg/(m·s$^3$) |
| $P$ | pressure, Pa | $m$ | mass, kg |
| $\rho$ | density, kg/m$^3$ | $e$ | normal restitution coefficient |
| $\mu$ | friction coefficient | | |

## REFERENCES

Bakshi, A., Altantzis, C., Ghoniem, A. F. 2014. Towards accurate three-dimensional simulation of dense multi-phase flows using cylindrical coordinates. Powder Technology 264, 242-255.

Cranfield, R. R., Geldart, D. 1974. Large particle fluidisation. Chemical Engineering Science 29(4), 935-947.

Forterre, Y., Pouliquen, O. 2008. Flows of dense granular media. Annual Review of Fluid Mechanics. 40, 1-24.

Gilliland, E. R., Mason, E. A. 1949. Gas and solid mixing in fluidized beds. Industrial & Engineering Chemistry 41(6), 1191-1196.

Gidaspow, D. 1994. Multiphase flow and fluidization: continuum and kinetic theory descriptions. Academic Press, New York, USA.

Goldhirsch, I. 2003. Rapid granular flows. Annual Review of Fluid Mechanics 35(1), 267-293.
Jenkins, J. T., Zhang, C. 2002. Kinetic theory for identical, frictional, nearly elastic spheres. Physics of Fluids 14, 1228-1235.
Kuipers, J. A. M., van Duin, K. J., van Beckum, F. P. H., van Swaaij, W. P. M. 1992. A numerical model of gas-fluidized beds. Chemical Engineering Science 47, 1913.
Lu, H. L., Gidaspow, D. 2003. Hydrodynamics of binary fluidization in a riser: CFD simulation using two granular temperatures. Chemical Engineering Science 58, 3777-3792.
Li, T., Grace, J., Bi, X. 2010. Study of wall boundary condition in numerical simulations of bubbling fluidized beds. Powder Technology 203(3), 447-457.
Laverman, J. A., Fan, X., Ingram, A., van Sint Annaland, M., Parker, D. J., Seville, J. P. K., & Kuipers, J. A. M. 2012. Experimental study on the influence of bed material on the scaling of solids circulation patterns in 3D bubbling gas–solid fluidized beds of glass and polyethylene using positron emission particle tracking. Powder Technology 224, 297-305.
Pouliquen, O., Chevoir, F. (002. Dense flows of dry granular material. Comptes Rendus Physique 3(2), 163-175.
Roux, J. N., Combe, G. 2002. Quasistatic rheology and the origins of strain. Comptes Rendus Physique, 3(2), 131-140.
Srivastava, A., Sundaresan, S. 2003. Analysis of a frictional–kinetic model for gas–particle flow. Powder Technology 129(1), 72-85.
Taghipour, F., Ellis, N., Wong, C. 2005. Experimental and computational study of gas–solid fluidized bed hydrodynamics. Chemical Engineering Science 60(24), 6857-6867.
Verma, V., Deen, N. G., Padding, J. T., Kuipers, J. A. M. 2013. Two-fluid modeling of three-dimensional cylindrical gas–solid fluidized beds using the kinetic theory of granular flow. Chemical Engineering Science 102, 227-245.
Yang L., Padding J. T., Kuipers J. A. M. 2016a. Modification of Kinetic Theory for Frictional Spheres, Part I: Two-fluid model derivation and numerical implementation. Chemical Engineering Science 152, 767-782.
Yang L., Padding J. T., Kuipers J. A. M. 2016b. Modification of Kinetic Theory of Granular Flow for Frictional Spheres, Part II: Model validation. Chemical Engineering Science 152, 152: 783-794.
Yang L., Padding J. T., Kuipers J. A. M. 2016c. Partial slip boundary conditions for collisional granular flows at flat frictional walls. AIChE Journal.